# Supplementary Information for

# Evidence of Donor-Acceptor Pair Transition-Induced Quantum Emitters in Hexagonal Boron Nitride

Qing-Hai Tan[1,2,3#], Jia-Min Lai[1,2#], Xue-Lu Liu[1,2], Dan Guo[1,2], Yong-Zhou Xue[1,2], Xiu-Ming Dou[1,2], Bao-Quan Sun[1,2], Hui-Xiong Deng[1,2], Ping-Heng Tan[1,2,4,5], Igor aharonovich[6,7]*, Wei-Bo Gao[3*], Jun Zhang[1,2,4,5]*

[1] State Key Laboratory of Superlattices and Microstructures, Institute of Semiconductors, Chinese Academy of Sciences, Beijing 100083, China

[2] Center of Materials Science and Optoelectronics Engineering, University of Chinese Academy of Sciences, Beijing 100049, China

[3] Division of Physics and Applied Physics, School of Physical and Mathematical Sciences, Nanyang Technological University, 637371, Singapore

[4] Beijing Academy of Quantum Information Science, Beijing 100193, China

[5] CAS Center of Excellence in Topological Quantum Computation, University of Chinese Academy of Sciences, Beijing 101408, China

[6]School of Mathematical and Physical Sciences, University of Technology Sydney, Ultimo, 2007, New South Wales, Australia

7. ARC Centre of Excellence for Transformative Meta-Optical Systems; Faculty of Science University of Technology Sydney, NSW 2007 Australia

[#] These authors contributed equally

*Email: igor.aharonovich@uts.edu.au, wbgao@ntu.edu.sg, zhangjwill@semi.ac.cn

## Section I. DFT Calculations

Based on density functional theory (DFT)[1], we carried out first-principles calculations with the generalized Kohn-Sham scheme[2], as implemented in the Vienna ab-initio simulation package (VASP)[3]. An energy cut-off of 400 eV was used in the calculation. The convergence criterion for the forces is less than 0.02 eV/Å, and the change of the total energy is less than $10^{-5}$ eV. We carried out the screened hybrid functional of Heyd, Scuseria, and Ernzernof (HSE)[4,5] for the electronic structural calculations. In this method, the short-range exchange potential is calculated by mixing a fraction of nonlocal Hartree-Fock exchange with the generalized gradient approximation (GGA) of Perdew, Burke, and Ernzernof (PBE)[6]. The screening parameter was set to 0.2 $Å^{-1}$ and the mixing parameter α=0.31 was used in our calculation. This value of α closely corresponds to the experimental band gap of hBN. The defective systems were modeled with a 3×3×2 supercell for monolayer BN. And for bulk BN, a 6×6×1 supercell was used. The supercells were sampled with a 3×3×3 and 3×3×1 k-point mesh for bulk and monolayer BN, respectively. Native defects and

impurities are created by adding and removing atoms from the supercell. We should note that the energy of the host valence band maxima is set to zero here. At 4 K, the electron-phonon coupling is weak (almost no phonon sideband is observed in our spectra) and lattice relaxation hardly affects the calculation of defect energy levels, thus we did not consider the lattice relaxation[7].

## Section II: Supplementary Figures

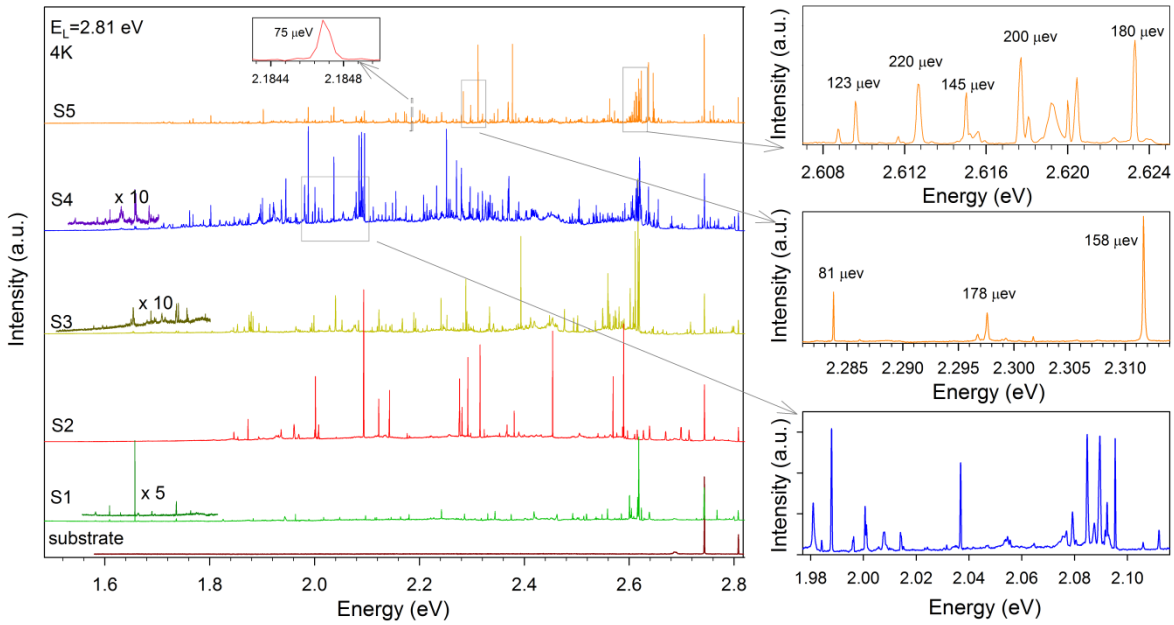


**Fig. S1** | (a) PL spectra of different hBN samples (labeled by S1-S5) with excitation wavelength 442 nm (2.81 eV) at 4K. (b-d). The zoomed-in PL range in (a).

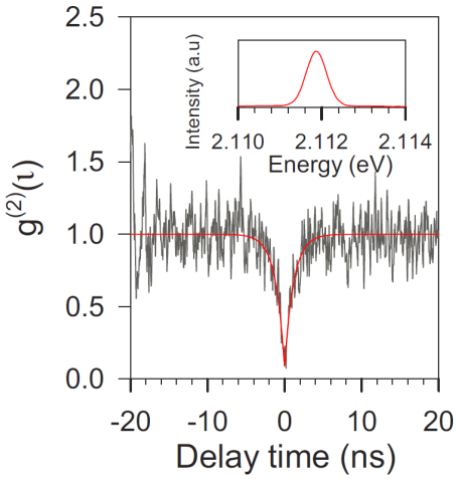


**Fig. S2** | The measurement result of the second-order correlation function for one PL peak at 4 K. The inset shows the corresponding PL spectrum.

.

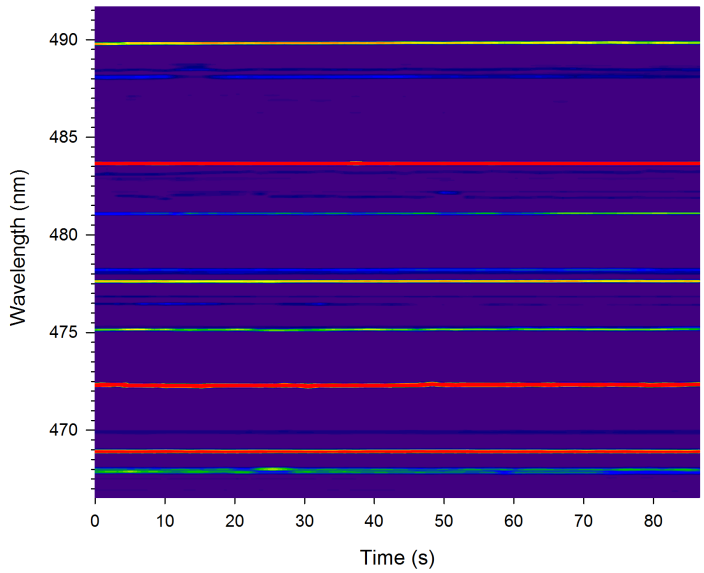


**Fig. S3** | The temporal evolution of different emitters under continuous illumination at 4K.

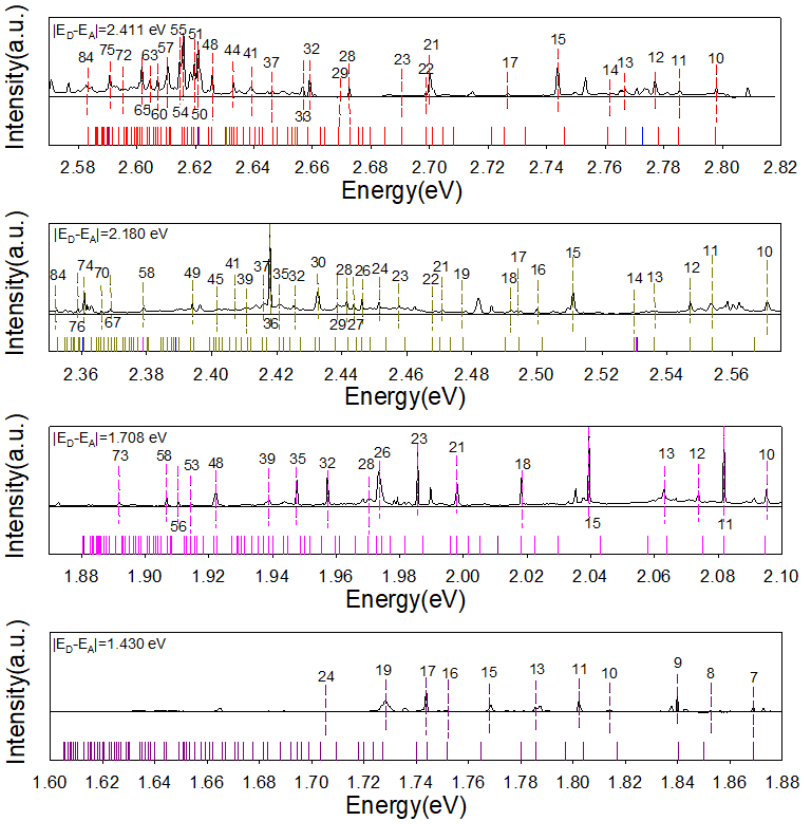


**Fig. S4** | The calculated DAP lines based on *type 1* transition.

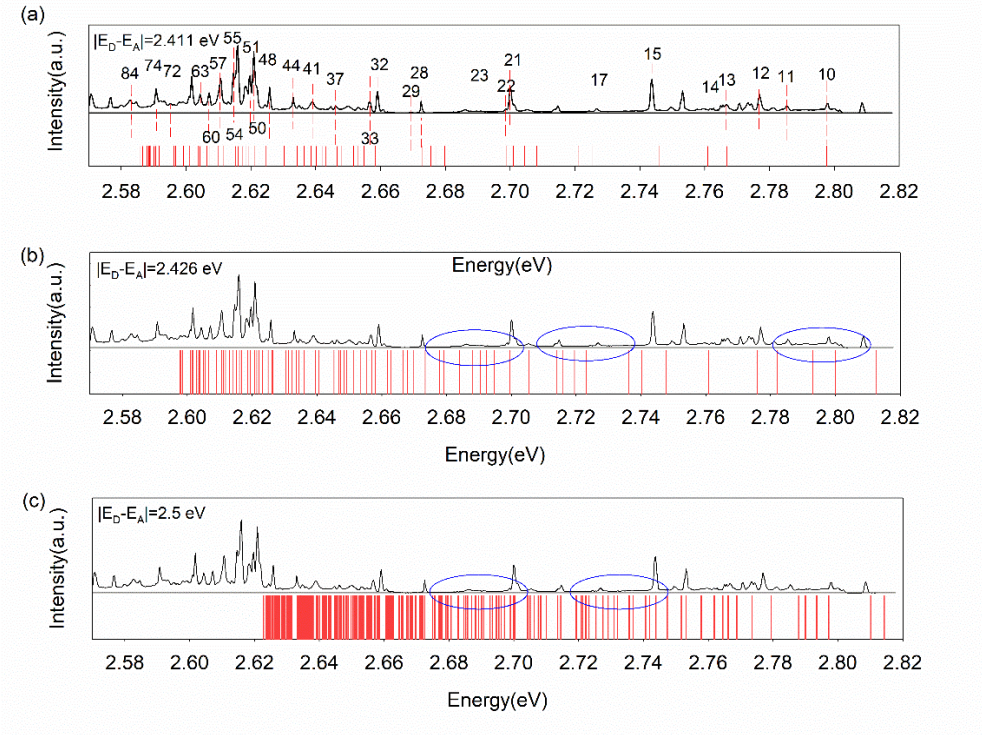


**Fig. S5** | The calculated *type 1* DAP lines based on different $|E_D-E_A|$.

We display three fitting results with different $|E_A-E_D|$ in Fig. S5. Obviously, the deviation between the calculated values and the experimental results in Fig. S5 (b) and (c) is larger than that in Fig. S5(a), especially in the small shell number region (labeled by the blue oval). Thus, the value of $|E_A-E_D|$ is selected specially.

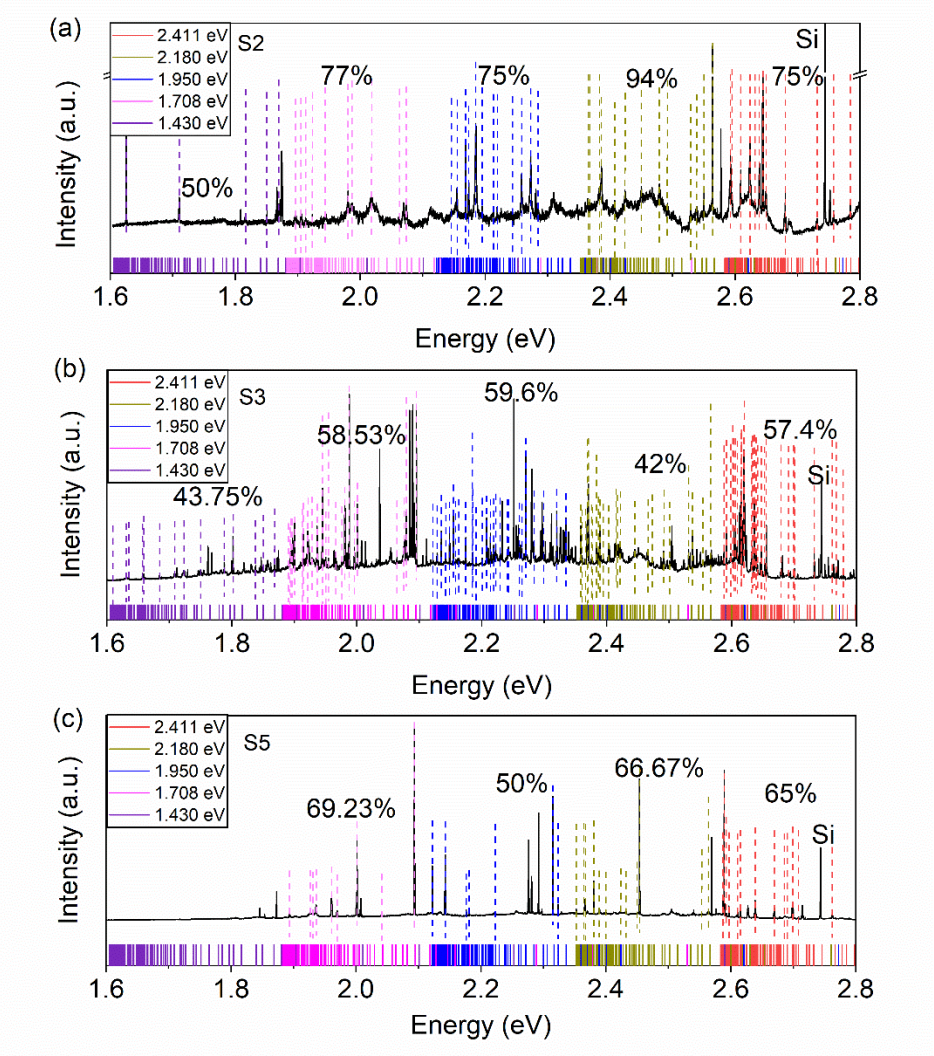


**Fig. S6**| The calculated DAP lines based on *type 1* for different samples.

We measured different nanoflakes at 4 K and they all show lots of similar sharp lines covering from 450~750 nm though the peak distribution may be slightly biased due to the uneven distribution of defects and stress. We use the same $|E_A\text{-}E_D|$ value to match these spectra and find that most of the lines can be fitted well, as shown in Fig. S8.

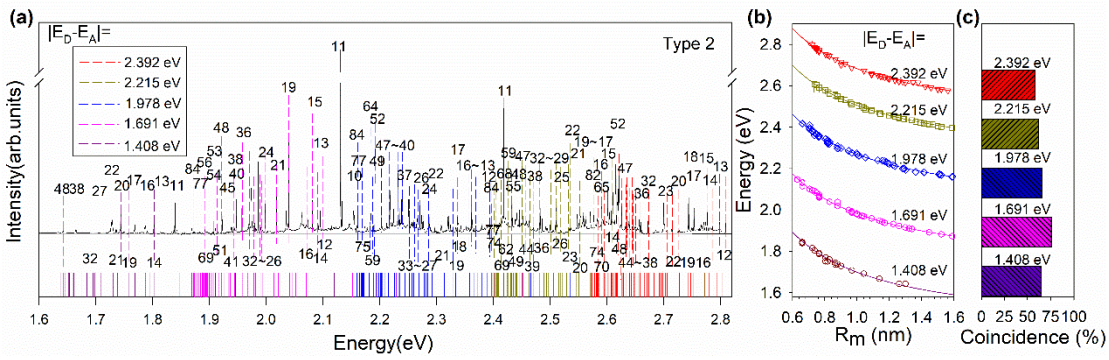

**Fig. S7**| (a) The calculated spectral distribution of *type2* DAPs. (b) The calculated emitted-photon energies based on the DAP model as a function of Rm (the distance between the donors and acceptors, where m is the shell numbers). The solid symbols are experimental results and the solid curves are the calculated results of *type 2* based on equation 1. (c) The coincidence of experimental lines that match the calculated DAP lines overall measured PL lines in each range.

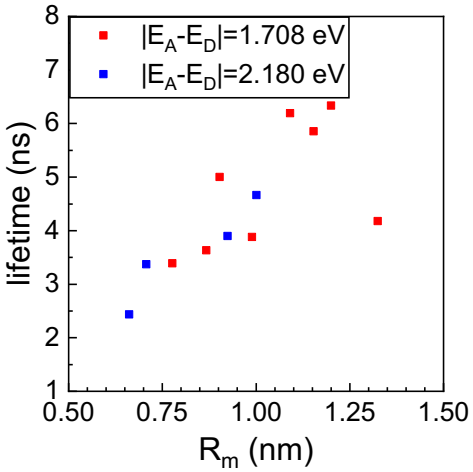


**Fig. S8**| Two group $R_m$-dependent DAP lifetimes fitted by *type 1*.

The DAP lifetime of shallow impurities is dependent on the overlap of donor and acceptor's wavefunctions and can be expressed as[8-10]:$\tau(R_m)^{-1} \propto \exp(-2R_m / a_e)$, where $R_m$ is the distance between the donor and acceptor, $a_e$ is the donor Bohr radium. This form was based on the effective mass approximation and hydrogen-like model. For shallow impurities, the Bohr radium extent is much greater than the crystal constant of the host materials, and thus the DAP lifetime can vary by one or more magnitude with the distance between donor and acceptor changed[10-14]. Besides, other factors may influence the DAP radiative recombination, such as concentrations[10] and nonradiative process[15], resulting in the relationship between lifetime with $R_m$ will deviate from this formula.

In our case, the impurities in hBN are deep-level defects, whose Bohr radius is much smaller than that of the shallow levels. i.e., just extent to several protocells. Therefore, there are no grounds for assuming a Coulomb field for the center with correction for the dielectric constant and using the effective-mass approximation[16]. We measured the PL decay of the donor-acceptor pairs in our hBN sample and extract DAP lifetime in two groups whose $|E_D - E_A|$ equals 2.180 eV and 1.708 eV in Fig. S4. The lifetimes of the DAP transition increase linearly with the increasing $R_m$. The resolution of 600 lines $mm^{-1}$ grating and 550 mm focal length we used in the life measurement is much lower than 2400 lines $mm^{-1}$ grating and 800 mm focal length used in the spectral measurement in the manuscript, so if the two peaks are too close to distinguish them, and then these decay channels interact with each other, resulting in inaccurate lifetime measurement. In addition, the factors mentioned above that influence the lifetime of shallow level impurities may also exist in our experiment. In conclusion, the life measurement results support "more

distant pairs should give longer lifetimes", but not the exponential relationship as with the shallow level impurities. Therefore, it is difficult to obtain the dependence of the lifetime of deep level DAP on $R_m$ from the existing experimental results now.

## Section III: DFT calculated results

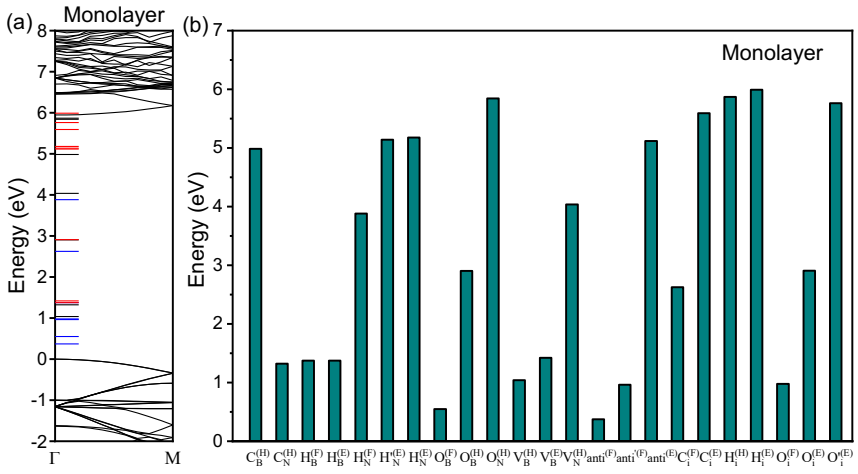


**Fig. S9**| (a) The calculated band structure of the monolayer hBN and the energy levels of different defect types. The blue lines indicate these defect states which are full-filled with electrons, the black straight lines represent these defect states which are half-filled with electrons, and these red lines denote the empty defect states. The energy of the host valence band maxima is set to zero. (b) The energy of different defect types. The green columns represent defects in the monolayer hBN case, and the white columns represent defects in the bulk hBN case. The superscript (F), (H), and (E) indicate the defect states are full-filled with electrons, half-filled with electrons, and empty, respectively. (An apostrophe (') is used to distinguish some substitutional atoms with the same electron occupancy two energy levels). For example, $C_B^{(H)}$ denotes a C impurity substituting for a lattice B atom and half-filled with electrons. Anti-site denotes $B_N$ and $N_B$, $V_B$ and $C_i$ denote boron vacancy and carbon interstitial, respectively.

Fig. S9 shows the electronic energy band structures of the monolayer hBN and its possible defect states calculated by DFT. The defect types in monolayer and bulk hBN are almost the same, but the energies have a small difference, indicating the energy is small varied in different thickness hBN for the same defect type.

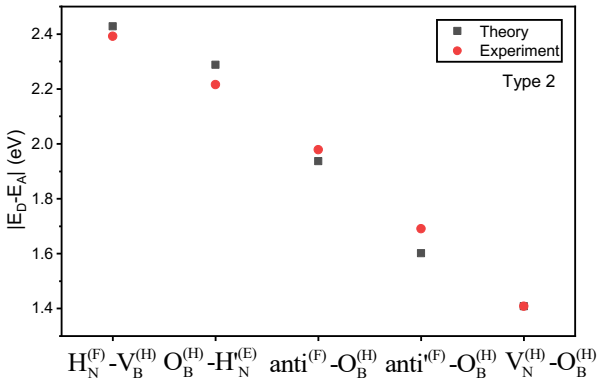


**Fig. S10**| The $|E_D\text{-}E_A|$ of different *type2* DAPs from our fitting result (red circle) and DFT calculation (black square).

## Section IV: Temperature dependence of linewidth and PL peak positions.

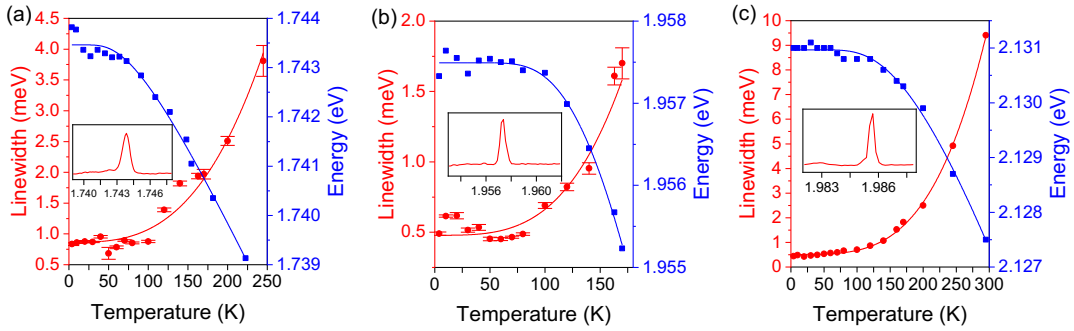


**Fig. S11**| (a) (b) (c) The temperature dependence of linewidth and energy of the PL peaks with different peak energies. The inset shows the PL peaks.

---

**References**


1 Hohenberg, P. & Kohn, W. Inhomogeneous Electron Gas. *Physical Review* **136**, B864-B871, doi:10.1103/PhysRev.136.B864 (1964).

2 Kohn, W. & Sham, L. J. Self-Consistent Equations Including Exchange and Correlation Effects. *Physical Review* **140**, A1133-A1138, doi:10.1103/PhysRev.140.A1133 (1965).

3 Kresse, G. & Furthmüller, J. Efficiency of ab-initio total energy calculations for metals and semiconductors using a plane-wave basis set. *Computational Materials Science* **6**, 15-50, doi: 10.1016/0927-0256(96)00008-0 (1996).

4 Heyd, J., Scuseria, G. E. & Ernzerhof, M. Hybrid functionals based on a screened Coulomb potential. *The Journal of Chemical Physics* **118**, 8207-8215, doi:10.1063/1.1564060 (2003).

5 Heyd, J., Scuseria, G. E. & Ernzerhof, M. Erratum: "Hybrid functionals based on a screened Coulomb potential" [J. Chem. Phys. 118, 8207 (2003)]. *The Journal of Chemical Physics* **124**, 219906, doi:10.1063/1.2204597 (2006).

6 Perdew, J. P., Burke, K. & Ernzerhof, M. Generalized Gradient Approximation Made Simple. *Physical Review Letters* **77**, 3865-3868, doi:10.1103/PhysRevLett.77.3865 (1996).

7 Tawfik, S. A. *et al.* First-principles investigation of quantum emission from hBN defects.

*Nanoscale* **9**, 13575-13582, doi:10.1039/C7NR04270A (2017).

8 Ohishi, M. Time-Resolved Studies on Recombination Luminescence of Donor-Acceptor Pairs in ZnSe. *Japanese Journal of Applied Physics* **25**, 1546-1551, doi:10.1143/jjap.25.1546 (1986).

9 Merz, J. L., Nassau, K. & Shiever, J. W. Pair Spectra and the Shallow Acceptors in ZnSe. *Physical Review B* **8**, 1444-1452, doi:10.1103/PhysRevB.8.1444 (1973).

10 Thomas, D. G., Hopfield, J. J. & Augustyniak, W. M. Kinetics of Radiative Recombination at Randomly Distributed Donors and Acceptors. *Physical Review* **140**, A202-A220, doi:10.1103/PhysRev.140.A202 (1965).

11 Nakashima, S. & Nakamura, A. Radiative recombination of donor-acceptor pairs in ZnTe. *Solid State Communications* **38**, 1289-1292, doi:10.1016/0038-1098(81)91008-5 (1981).

12 Dang, L. S. & Romestain, R. Luminescence decay of distant donor-acceptor pairs in phosphorous-doped ZnTe. *Solid State Communications* **43**, 829-831, doi: 10.1016/0038-1098(82)90849-3 (1982).

13 Bäume, P., Strauf, S., Gutowski, J., Behringer, M. & Hommel, D. Analysis of time-resolved donor—acceptor-pair spectra of ZnSe : Li and ZnSe : N. *Journal of Crystal Growth* **184-185**, 531-535, doi: 10.1016/S0022-0248(98)80110-3 (1998).

14 Yi, G. J. & Neumark, G. F. Impurity radii: Evaluation from donor-acceptor pair luminescence and comparison to effective-mass values. *Physical Review B* **48**, 17043-17045, doi:10.1103/PhysRevB.48.17043 (1993).

15 Kamiya, T. & Wagner, E. Shallow acceptor binding energy and lifetime of donor-acceptor pairs in gallium arsenide. *Journal of Applied Physics* **47**, 3219-3223, doi:10.1063/1.323118 (1976).

16 Keldysh, L. Deep levels in semiconductors. *J Sov. Phys. JETP* **18**, 253 (1964).